

Ensuring Data Freshness for Blockchain-enabled Monitoring Networks

Minsu Kim, Sungho Lee, Chanwon Park, Jemin Lee, *Member, IEEE*, and Walid Saad, *Fellow, IEEE*

Abstract—The age of information (AoI) is a recently proposed metric for quantifying data freshness in real-time status monitoring systems where timeliness is of importance. In this paper, the problem of characterizing and controlling the AoI is studied in the context of blockchain-enabled monitoring networks (BeMN). In BeMN, status updates from sources are transmitted and recorded in a blockchain. To investigate the statistical characteristics of the AoI in BeMN, the transmission latency and the consensus latency are first rigorously modeled. Then, the average AoI, the AoI violation probability, and the peak AoI violation probability are derived in a closed form so as to quantify the performance of BeMN. Furthermore, a simplified form is derived for the AoI violation probability, and it is shown that this quantity can capture the upper or lower bound of the actual AoI violation probability. Simulation results show that each BeMN parameters (i.e., target successful transmission probability, block size, and timeout) can have conflicting effects on the AoI-related performance. Subsequently, design insights are provided to maintain the freshness of the status data in BeMN. Then, experimental results with a real Hyperledger Fabric platform further validate the accuracy of our modeling and analysis.

Index Terms—Age of information, blockchain, Hyperledger Fabric, latency, stochastic geometry

I. INTRODUCTION

The emergence of blockchains has ushered in a new breed of decentralized data management platforms that have been adopted in a broad range of real-time wireless Internet of Things (IoT) monitoring applications ranging from healthcare systems to pollution detection and autonomous factories [2]. In such real-time monitoring systems, data integrity is one of the important requirements in order to prevent unintended or malicious changes in the data. Through integration with blockchains, real-time monitoring systems can maintain data integrity in a distributed manner without the need for a central authority. Although blockchains can provide a secure data management platform for monitoring systems by ensuring data integrity, they cannot guarantee data freshness. The use of outdated data when making system-wide decisions, such as raising an alarm due to a high temperature or level of

pollution, can lead to incorrect outputs. Those outputs can further jeopardize the operation of a whole system. Therefore, it is of importance to maintain fresh data for blockchain-enabled monitoring systems to prevent undesired outputs.

To quantify the degree of data freshness, the notion of age of information (AoI) has been proposed in [3]. The AoI is defined as the elapsed time from the generation of the latest received status update. Several variants of the AoI recently appeared, including the so-called peak AoI (PAoI), which measures the largest staleness of information [4]. In blockchain-enabled monitoring systems, status updates are recorded in distributed ledgers. Hence, the AoI can be used as a suitable metric to quantify data freshness in the ledgers of a blockchain. However, in order to optimize the AoI and maintain data freshness in a blockchain, several challenges must be addressed such as accounting for the transaction processing latency to update ledgers.

There has been a number of prior works that looked at the measurement and analysis of transaction processing latency in blockchain platforms [5]–[8]. The authors in [5] and [6] implemented a permissioned blockchain integrated IoT platform as a proof of concept for monitoring networks, and they evaluated the performance of the proposed networks in terms of latency. The work in [7] investigated the effects of block generation frequency on the end-to-end latency in Ethereum-based blockchain platforms under cellular and Wi-Fi networks. The authors in [8] studied the effects of the number of network hops and replica nodes on the end-to-end latency in Byzantine fault tolerance-based blockchain platforms. Although the latency for a status update in blockchain platforms is studied and evaluated in [5]–[8], data freshness was not characterized. For maintaining data freshness in blockchain-enabled networks, one must consider jointly the latency in processing transactions, the transaction generation frequency, and the communication latency.

Recently, in [9], the authors analyzed data freshness, in terms of average AoI, for a public blockchain and the IOTA platform. However, the distribution of the AoI is not studied although it is essential to show the percentage of the time guaranteeing a certain target AoI. Moreover, the latency to process a transaction is simply modeled to follow an exponential distribution, without the validation in a real blockchain platform. We also acknowledge that a number of works [10]–[15] looked at different aspects related to the analysis and optimization of the AoI and PAoI in monitoring networks. Moreover, the work in [16] quantified the worst-case achievable PAoI for an augmented reality system over future wireless networks. However, these prior works do not investigate the synergies

M. Kim, S. Lee, C. Park, and J. Lee are with the Department of Information and Communication Engineering, Daegu Gyeongbuk Institute of Science and Technology, Daegu, South Korea, 42988 (e-mail: {kms0603, seuho2003, pcw0311, jmnlee}@dgist.ac.kr).

W. Saad is with the Wireless@VT Group, Bradley Department of Electrical and Computer Engineering, Virginia Tech, Blacksburg, VA 24061 USA (e-mail: walids@vt.edu).

The material in this paper will be presented, in part, at the IEEE International Conference on Communications, Montreal, Canada, Jun. 2021 [1].

This research was supported, in part, by the U.S. Office of Naval Research (ONR) under MURI Grant N00014-19-1-2621.

between blockchains and AoI, especially for a *permissioned blockchain*. Note that a permissioned blockchain can be more suitable for the data management in IoT platforms than a public blockchain as it avoids the use of an intensive consensus protocol (e.g., mining) under a strict membership rule.

The main contribution of this paper is, thus, a novel framework to analyze the data freshness of monitoring networks that use a permissioned blockchain for data management. We call such networks blockchain-enabled monitoring networks (BeMN), and it consists of sources, base stations (BSs), and an Hyperledger Fabric (HLF) [17], which is one of the most widely used permissioned blockchain platform [18]. In BeMN, sources monitor physical phenomena, and each source transmits its monitored data to an associated BS, which is connected to the HLF network. Following the consensus process in the HLF network, the monitored data is stored in distributed ledgers, and this newly monitored data is used as a status update of the source. To measure the freshness of data in BeMN, we analyze the distribution of the PAoI and the average AoI of BeMN by considering both the transmission latency and the consensus latency. We then obtain the AoI violation probability, which captures the probability that the AoI exceeds a target AoI. Furthermore, we explore the effects of communication and HLF parameters on the average AoI, the PAoI violation probability, and the AoI violation probability. Our main contributions can thus be summarized as follows.

- We characterize, in a closed-form, the statistical characteristics of the AoI for BeMN including the average AoI, the PAoI violation probability, and the AoI violation probability by considering the consensus latency in an HLF network as well as the transmission latency.
- We explore the impacts of the communication parameter (i.e., target successful transmission probability (STP)) and the HLF parameters (i.e., block size and timeout) on the AoI in BeMN. In particular, simulation results show that each BeMN parameter can have conflicting effects on the AoI-related performance. Hence, a higher target STP or a larger value for the HLF parameters will not always guarantee a lower AoI.
- We implement a real HLF platform (v1.3) for measuring the consensus latency. We then validate the accuracy of our modeling and analysis through the implemented HLF platform. Experimental results also corroborate the impacts of the BeMN parameters on the AoI-related performance.

The rest of this paper is organized as follows. Section II introduces the overall transaction flow in an HLF and the associated parameters. Section III describes the HLF blockchain-enabled monitoring network and models the consensus latency. Section IV derives the distribution of the PAoI, the average AoI, and the AoI violation probability in BeMN. Section V provides the validation of the analytical results and effects of the parameters of BeMN on the AoI violation probability. Finally, conclusions are drawn Section VI.

Notation: An overview of our notation is shown in Table I.

TABLE I. Summary of our key notations.

Notation	Definition
B	Block size of an HLF network
T	Timeout of an HLF network
α	Shape parameter of the Gamma distribution
β	Rate parameter of the Gamma distribution
λ_s	Spatial density of sources
λ	Spatial density of BSs
P	Transmission power of sources
n	Pathloss exponent
$\bar{\epsilon}$	Maximum target data rate
ζ	Target STP
D	Packet size
T_{int}	Inter-generation time of two consecutive packets that successfully arrive at the BS
ρ_s	Generation rate of packets at a source
ρ	Generation rate of packets that successfully arrive at the BS
$T_{\text{tot},k}$	Total latency of packet k to update status
X_k	Consensus latency of packet k
T_{tx,x_0}	Transmission latency
$T_{\text{eff},k}$	Inter-generation time of two effective packets $k-1$ and k
G_k	Generation instant of effective packet k
A_k	Arrival instant of effective packet k at the BS
U_k	Update instant of effective packet k
$\Delta_{p,k}$	Peak AoI of effective packet k
v	Target AoI
T_k^v	Time duration of the AoI being larger than v between U_k and U_{k-1}
T_{v,x_0}	Time difference between v and T_{tx,x_0}
$\bar{\Delta}$	Average AoI
P_v	AoI violation probability
P_{pv}	PAoI violation probability

II. HYPERLEDGER FABRIC: PRELIMINARIES

In this subsection, we present the overall structure of HLF and the components of the consensus process for a status update. We also introduce the HLF parameters which affect the performance of BeMN.

A. HLF Transaction Flow

HLF is a permissioned blockchain platform, in which all changes made by transactions are committed to the distributed ledger [17]. In HLF, peer nodes (or peers) hold their own copies of the distributed ledgers. The ledger is a key-value database, which consists of two parts: a blockchain and a world state. In the blockchain, the immutable records of status

changes are stored. Meanwhile, the world state is also a database, in which the current value of the status is paired with its own key and current version number. Hence, all data in the ledger is identified by its own key and version number. Every ledger update starts with the generation of a transaction. A *transaction* is executed against the specified function to update the stored data in the ledger with each corresponding key. Here, we assume that the IoT monitoring system's sources generate a transaction to update their status as done in [5] and [6]. In HLF, participants are all identified. Therefore, the costly consensus method used in public blockchains, known as mining, is not necessary. Instead, the consensus process in HLF is composed of three phases: endorsement phase, ordering phase, and validation phase are described next and detailed [19] and [20].

1) *Endorsement Phase*: All transactions for status updates enter the endorsement phase first. During this phase, peers simulate a transaction using their ledgers. The peers make sure that they have identical simulation results, which are called endorsements. These endorsements include the updated status and version number of the ledger in the peer. Then, the transaction with the endorsements is transmitted to the ordering node. Note that, although the transaction simulation results are ready, the status is not updated in this phase.

2) *Ordering Phase*: The ordering phase is used not only to arrange transactions in a chronological order but also to generate new blocks with the ordered transactions. The ordering nodes continuously include transactions into a new block until it reaches the pre-defined maximum block size. In order to avoid high latency, a timer is prepared with a pre-defined timeout value. If the timer expires, the nodes instantly export the new block, regardless of the current number of transactions in the block. The newly generated block is then delivered to the peers by the ordering nodes.

3) *Validation Phase*: Next, in the validation phase, the blocks that are delivered to the peers will be validated and the ledger will be updated. This phase consists of two sequential steps: verification and update. The peers investigate if each transaction in the block is properly endorsed from the endorsement phase. Then, the peers check whether the version numbers in the endorsements are identical to the ones currently stored in their copied ledgers. This verification is also called the multi-version concurrency check (MVCC) verification. Note that the version number increases each time the corresponding status is updated. Hence, if the two version numbers are different, then this signifies that the status has already been updated by the previous transaction before the current one completes the consensus process. If the version numbers are different, then the transaction becomes invalid and ineffective. Finally, the peers update the world state and the blockchain in the ledger.

B. HLF Parameters

We are interested in two key HLF parameters: the block size and the block-generation timeout, which essentially refer to the HLF configurations. As introduced in the ordering phase section, those parameters control how long a transaction will wait in the ordering phase, which affects the consensus latency.

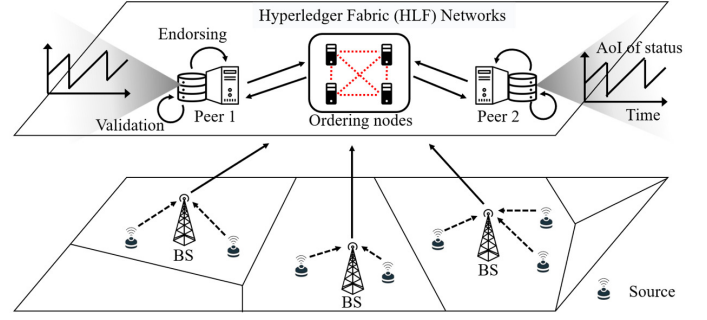


Fig. 1. BeMN structure, composed of sources, BSs, and the HLF network.

Hence, for maintaining data freshness in monitoring networks, these parameters should be properly designed to avoid a large waiting time in the ordering phase.

1) *Block Size, B* : A block size B limits the maximum number of transactions in a block. A newly arrived transaction needs to wait in the ordering phase until the number of transactions in the block reaches B . Therefore, a larger B will lead to longer waiting times for the transactions because more time is needed to fill up the block.

2) *Timeout, T* : A timeout T is another way to limit the waiting time of a transaction in the ordering phase. The transaction can wait up to the timeout value T for other transactions in the ordering phase. The new block can move to the next phase even if the block is not completely full to avoid long latency. As expected, transactions generally need to wait longer as T increases.

Given these preliminaries, in the following section, we present our system model based on Section II.

III. BLOCKCHAIN-ENABLED MONITORING NETWORK

A. System Model

We consider BeMN composed of sources, BSs, and an HLF network. In BeMN, the sources monitor physical phenomena (e.g., temperature, pollution level) and update the corresponding status stored in the HLF as shown in Fig. 1. We assume that the distribution of the sources follows a homogeneous Poisson point process (HPPP) Φ_s with spatial density λ_s . The source transmits a packet through a wireless uplink channel to the nearest BS as done in [21] and [22]. We assume that all the sources use the same transmission power P . The distribution of the BSs also follows an HPPP Φ_m with spatial density λ . Without loss of generality, we consider a typical source located at the origin and its associated BS at x_0 . Each channel is allocated to one source only in the cell of any given BS to mitigate intra-cell interference between sources belonging to the same cell.

We assume the BSs to be connected to the HLF network, whereby each status information of the source is stored with its key values. As shown in Fig. 1, a source monitors a physical phenomenon and generates a packet with newly observed information. In our model, the source generates a packet with an exponentially distributed inter-generation time and rate ρ_s as done in [23] and [24]. The packet is delivered to the HLF

via a BS in the form of a transaction. Successfully received transactions can update their status information through the consensus process described in Section II-A.

We define the consensus latency as the total time required for the commitment of a transaction, which is the sum of the latencies in each phase. Then, the total latency of packet k will be:

$$T_{\text{tot},k} = X_k + T_{\text{tx},x_o,k}, \quad (1)$$

where X_k is the consensus latency of packet k and $T_{\text{tx},x_o,k}$ is the transmission latency needed to send a packet from the typical source to its associated BS. The consensus latency $\{X_k, k \geq 1\}$ is assumed to be independent and identically distributed (i.i.d.).

B. Consensus Latency Modeling

We now model the consensus latency in our BeMN. From the empirical results of a constructed HLF platform, it is shown in [25] that the Gamma distribution is reasonable for modeling the consensus latency in the HLF platform. Hence, the consensus latency X_k of packet k can be modeled as a Gamma random variable, i.e., $X_k \sim \text{Gamma}(\alpha, \beta)$, whose probability density function (PDF) is given by [26]

$$f_{X_k}(x) = \frac{\beta^\alpha}{\Gamma(\alpha)} x^{\alpha-1} e^{-\beta x}, \quad (2)$$

where α and β are the shape and the rate parameters, respectively, and $\Gamma(\cdot)$ is a Gamma function. To determine the values of α and β , we use the maximum likelihood estimation [26]. Specifically, α and β can be given by

$$\alpha = \frac{1}{4A} \left(1 + \sqrt{1 + \frac{4A}{3}} \right), \beta = \frac{\alpha}{\bar{X}}, \quad (3)$$

where \bar{X} is the mean of consensus latencies, and A is given by

$$A = \log(\bar{X}) - \sum_{i=1}^N \log(X_i)/N \quad (4)$$

for the sample consensus latency X_i and N number of samples. We use the Kolmogorov-Smirnov (KS) test as done in [27] and [28] to quantify the accuracy of the modeling (the accuracy results are given in Section V). Note that this modeling of consensus latency is applicable to general HLF with version 1.0 or higher.¹

C. Transmission Latency

Next, we analyze the transmission latency $T_{\text{tx},x_o,k}$ of BeMN. The signal-to-interference-plus-noise ratio (SINR) received by a BS located at point x_o under Rayleigh fading channel is

$$\gamma_{x_o} = \frac{Ph_{x_o}l^{-n}}{I_{x_o} + N_0W}, \quad (5)$$

where h_{x_o} is the fading channel gain, i.e., $h_{x_o} \sim \exp(1)$, l is the distance between the typical source and the associated BS, n is the path loss exponent, N_0 is the noise power, and W is the channel bandwidth. In (5), I_{x_o} is the inter-cell interference

from other sources that use the same uplink frequency band, given by

$$I_{x_o} = P \sum_{u \in \Psi_u} h_{u,x_o} \|u\|^{-n}, \quad (6)$$

where Ψ_u denotes the set of locations of the interfering sources which use the same frequency band with the typical source. We assume that each cell has one source that uses the same uplink frequency band as the typical source. Hence, the density of interfering sources is the same as that of the BSs, λ . Then, the achievable data rate R_{x_o} is given by

$$R_{x_o} = W \log_2(1 + \gamma_{x_o}). \quad (7)$$

We define STP p_c as the probability that the achievable data rate R_{x_o} is greater than or equal to a target rate ϵ , i.e., $p_c = \mathbb{P}[R_{x_o} \geq \epsilon]$. We assume that a packet is transmitted at the maximum target rate $\bar{\epsilon}_{x_o}$ to guarantee $p_c \geq \zeta$, where ζ is a target STP. Hence, $\bar{\epsilon}_{x_o}$ is given by [29]

$$\bar{\epsilon}_{x_o} = \max \{ \epsilon \mid \mathbb{P}[R_{x_o} \geq \epsilon] \geq \zeta \}. \quad (8)$$

Then, $\bar{\epsilon}_{x_o}$ in (8) can be obtained in the following proposition.

Proposition 1. The maximum target rate $\bar{\epsilon}_{x_o}$ is the one that satisfies the following equation

$$\exp \left(-\frac{l^n}{P} N_0 W \theta(\bar{\epsilon}_{x_o}) - \frac{2\lambda\pi^2 l^2 \theta(\bar{\epsilon}_{x_o})^{2/n}}{nP^{2/n} \sin(2\pi/n)} \right) = \zeta, \quad (9)$$

where $\theta(\bar{\epsilon}_{x_o}) = 2^{\bar{\epsilon}_{x_o}/W} - 1$.

Proof. See Appendix (A). \square

From Proposition 1, we can see that finding a closed-form for $\bar{\epsilon}_{x_o}$ is challenging for a general path loss exponent. However, for $n = 4$, $\bar{\epsilon}_{x_o}$ can be derived as:

$$\bar{\epsilon}_{x_o} = W \log_2 \left[1 + \left\{ \frac{\sqrt{P}(-\pi^2\lambda + \sqrt{\pi^4\lambda^2 - 16N_0W \log \zeta})}{4N_0Wl^2} \right\}^2 \right]. \quad (10)$$

Since the source transmits a packet at the rate $\bar{\epsilon}_{x_o}$, the transmission latency T_{tx,x_o} can be defined as

$$\begin{aligned} T_{\text{tx},x_o} &= \frac{D}{\bar{\epsilon}_{x_o}} \\ &= \frac{D \log 2}{W} \left[1 + \left\{ \frac{\sqrt{P}(-\pi^2\lambda + \sqrt{\pi^4\lambda^2 - 16N_0W \log \zeta})}{4N_0Wl^2} \right\}^2 \right], \end{aligned} \quad (11)$$

where D [bits] is the packet size. Note that we omit the packet index k in T_{tx,x_o} since each packet experiences the same transmission latency when the source is at x_o .

In BeMN, each transmitted packet must go through the consensus process to complete an update. In contrast to conventional databases, in an HLF, this consensus latency is not negligible. Hence, we investigate the data freshness using AoI-related performance metrics, such as the average AoI, the AoI violation probability, and the PAoI violation probability, by considering both the transmission latency and the consensus latency in the following section.

¹HLF with version 1.0 or higher includes the MVCC verification

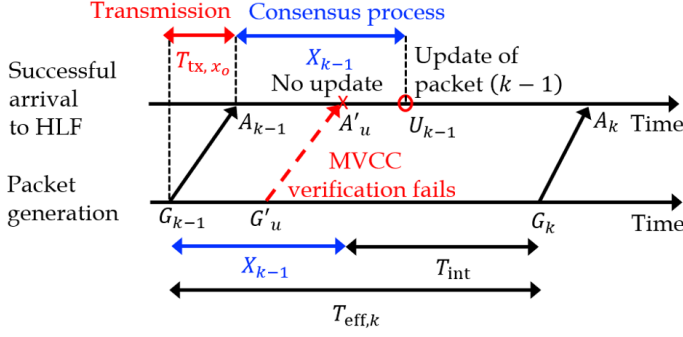


Fig. 2. MVCC verification failure of the packet generated at G'_u .

IV. AOI ANALYSIS OF BeMN

We now analyze the AoI violation probability in our BeMN. As a metric for measuring the data freshness, the AoI is defined as the elapsed time since the generation of the latest received packet [3]. We focus on the AoI of the specific status, which is stored with a certain key value in the ledger. As discussed in Section II, not every generated packet can make a valid update in BeMN because of the MVCC verification failure. If the status is updated before the current packet completes its consensus process, this packet becomes invalid and ineffective. We call the packets that make valid updates as *effective packets*. For effective packet k , we define G_k as the generation instant at the source, A_k as the arrival instant at the BS, and U_k as the update instant at the ledger. As shown in Fig. 2, packet k can be effective only if its arrival instant A_k is after U_{k-1} , which is the update instant of the previous effective packet $(k-1)$. All packets that arrive after X_{k-1} from G_{k-1} become effective packets. Then, the AoI at time t can be defined as

$$\Delta(t) = t - \max\{G_k \mid U_k \leq t\}. \quad (12)$$

In Fig. 2, G'_u and A'_u are, respectively, the generation instant and the arrival instant of invalid packet u . We also define the inter-generation time of two consecutive effective packets $T_{\text{eff},k} = G_k - G_{k-1}$.

The inter-generation time of two consecutive packets that successfully arrive at the BS from the source is denoted by T_{int} . Since the inter-generation time of packets follows an exponential distribution with rate ρ_s , T_{int} will also follow an exponential distribution with rate $\rho = \rho_s p_c$. We assume independence between T_{int} and $\{X_k, \forall k \geq 1\}$ in BeMN.² Due to the memoryless property of T_{int} , $T_{\text{eff},k}$ can be given as

$$T_{\text{eff},k} = X_{k-1} + T_{\text{int}}. \quad (13)$$

The PAoI is the AoI just before the update instant. As shown in Fig. 3, for effective packet k , PAoI is given by

$$\Delta_{p,k} = T_{\text{eff},k} + T_{\text{tot},k}. \quad (14)$$

²A dependence exists between T_{int} and $\{X_k, \forall k \geq 1\}$ due to the ordering phase in BeMN. However, this dependence is negligible as shown in Section V-A.

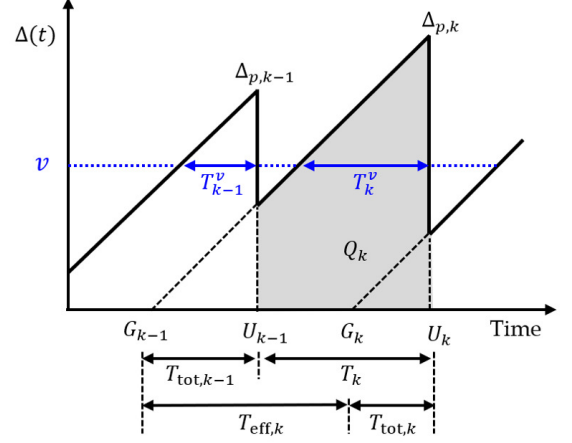


Fig. 3. A sample path of the AoI where G_k and U_k are the generation instant and the update instant of effective packet k .

From (13) and (14), we derive the average AoI $\bar{\Delta}$ of BeMN in the following lemma.

Lemma 1. In BeMN, the average AoI $\bar{\Delta}$ is given by

$$\bar{\Delta} = \frac{\rho\beta}{2(\alpha\rho + \beta)} \left(\frac{2}{\rho^2} + \frac{2\alpha}{\rho\beta} + \frac{\alpha^2 + \alpha}{\beta^2} \right) + \frac{\alpha}{\beta} + T_{\text{tx},x_o}, \quad (15)$$

where α and β are defined in (3), $\rho = \rho_s p_c$, and T_{tx,x_o} is given by (11).

Proof. Let Q_k be the area of the trapezoid between U_k and U_{k-1} as in Fig. 3. From [30], $\bar{\Delta}$ can be given by

$$\begin{aligned} \bar{\Delta} &= \lim_{T \rightarrow \infty} \frac{1}{T} \int_0^T \Delta(t) dt = \lim_{T \rightarrow \infty} \frac{1}{T} \sum_{k=1}^{N(T)} Q_k \\ &= \lim_{T \rightarrow \infty} \frac{N(T)}{T} \frac{1}{N(T)} \sum_{k=1}^{N(T)} Q_k \\ &\stackrel{(a)}{=} \lim_{T \rightarrow \infty} \frac{\sum_{k=1}^{N(T)} Q_k / N(T)}{\sum_{k=1}^{N(T)} (U_k - U_{k-1}) / N(T)} \\ &\stackrel{(b)}{=} \frac{\mathbb{E}[Q_k]}{\mathbb{E}[T_k]}, \end{aligned} \quad (16)$$

where $N(T)$ is the number of updates until time T , defined as $N(T) = \max\{k \mid U_k \leq T\}$. In (16), (a) follows from the fact that T can be presented in an infinite summation of the update intervals $U_k - U_{k-1}$ as T goes to infinity, and (b) follows from the ergodicity of the sample path.

In (16), we have: $Q_k = \frac{1}{2}(\text{PAoI}_k^2 - T_{\text{tot},k-1}^2)$. Therefore, using (14), $\mathbb{E}[Q_k]$ can be obtained as

$$\mathbb{E}[Q_k] = \frac{1}{2} \mathbb{E}[T_{\text{eff},k}^2 + 2T_{\text{eff},k}T_{\text{tot},k}]. \quad (17)$$

Using $T_{\text{eff},k}$ in (13), $\mathbb{E}[Q_k]$ can be represented as

$$\mathbb{E}[Q_k] = \frac{1}{2} \mathbb{E}[(T_{\text{int}} + X_{k-1})^2] + \mathbb{E}[(T_{\text{int}} + X_{k-1})(X_k + T_{\text{tx},x_o})]. \quad (18)$$

$$\begin{aligned}
P_v = & \frac{\rho\beta^{2\alpha+1}}{(\beta+\rho\alpha)\Gamma(\alpha)^2} \sum_{n=0}^{\infty} \frac{(\rho-\beta)^n}{n!(\alpha+n)\rho^{\alpha+n+1}} \left[\frac{\Gamma(\alpha+n+1)}{\beta^\alpha} \gamma(\alpha, \beta T_{v,x_0}) - \sum_{k=0}^{\infty} \frac{(-1)^k (\rho T_{v,x_0})^{\alpha+n+k+1}}{k! (\alpha+n+k+1)} B(\alpha+n+k+2, \alpha) \right. \\
& \times T_{v,x_0}^\alpha {}_1F_1(\alpha; 2\alpha+n+k+2; -\beta T_{v,x_0}) \left. \right] + \frac{\rho}{(\beta+\rho\alpha)\Gamma(\alpha)} \left\{ \alpha \gamma(\alpha, \beta T_{v,x_0}) - \sum_{n=0}^{\infty} \frac{(-\beta T_{v,x_0})^{2\alpha+n+1}}{n!\Gamma(\alpha)(\alpha+n+1)} B(\alpha+n+2, \alpha) \right. \\
& \times {}_1F_1(\alpha; 2\alpha+n+2; -\beta T_{v,x_0}) - (\beta T_{v,x_0})^{\alpha+1} B(\alpha, 2) T_{v,x_0}^\alpha {}_1F_1(\alpha; \alpha+2; -\beta T_{v,x_0}) \\
& \left. + \sum_{n=0}^{\infty} \frac{(-\beta T_{v,x_0})^{2\alpha+n+1}}{n!\Gamma(\alpha)(\alpha+n)} B(\alpha, \alpha+n+2) {}_1F_1(\alpha; 2\alpha+n+2; \beta T_{v,x_0}) \right\} + \frac{\Gamma(\alpha, \beta T_{v,x_0})}{\Gamma(\alpha)}. \quad (23)
\end{aligned}$$

Since $T_{\text{int}} \sim \text{Exp}(\rho)$ and $X_k \sim \text{Gamma}(\alpha, \beta)$, (18) can be given by

$$\mathbb{E}[Q_k] = \frac{2}{\rho^2} + \frac{2\alpha}{\rho\beta} + \frac{\alpha^2 + \alpha}{\beta^2} + \left(\frac{1}{\rho} + \frac{\alpha}{\beta} \right) \left(\frac{\alpha}{\beta} + T_{\text{tx},x_0} \right). \quad (19)$$

In (16), as shown in Fig. 3, T_k represents the interval of the update instants U_{k-1} and U_k , which can be given by

$$T_k = T_{\text{eff},k} + T_{\text{tot},k} - T_{\text{tot},k-1} = X_k + T_{\text{int}}. \quad (20)$$

Hence, we have $\mathbb{E}[T_k] = \frac{1}{\rho} + \frac{\alpha}{\beta}$. The average AoI $\bar{\Delta}$ can be then presented by substituting (19) and (20) into (16). \square

From Lemma 1, we can obtain $\bar{\Delta}$ in BeMN, which captures the overall freshness of status information stored in ledgers. To see whether a certain level of freshness is guaranteed in BeMN, we can evaluate the *AoI violation probability*, which is the probability that the AoI exceeds a target AoI v . The AoI violation probability P_v is given by [31]

$$P_v = \mathbb{P}[\Delta(t) \geq v] = \frac{\mathbb{E}[T_k^v]}{\mathbb{E}[T_k]}, \quad (21)$$

where T_k^v is the time duration during which the AoI is larger than v between the update instants U_{k-1} and U_k . Then, T_k^v is given by

$$\begin{aligned}
T_k^v &= \min \left\{ (\Delta_{p,k} - v)^+, T_k \right\} \\
&= \min \left\{ (X_{k-1} + X_k + T_{\text{int}} + T_{\text{tx},x_0} - v)^+, X_k + T_{\text{int}} \right\}, \quad (22)
\end{aligned}$$

where $(\cdot)^+ = \max(0, \cdot)$. We now obtain P_v of BeMN in the following theorem.

Theorem 1. In BeMN, the AoI violation probability P_v is given by (23) (see the top of the next page), where $T_{v,x_0} = (v - T_{\text{tx},x_0})^+$.

Proof. See Appendix B. \square

From Theorem 1, we can identify how the tail of the AoI distribution in BeMN is formed, which is not captured by $\bar{\Delta}$. This result can be used to prevent the status update AoI from being too stale. In Section V-A, we further show that the optimal value of the BeMN parameters to minimize P_v can be different from $\bar{\Delta}$.

We also obtain the AoI violation probability for the case of integer α in the following corollary.

Corollary 1. When the shape parameter α of the consensus latency distribution is an integer, the AoI violation probability P_v is given by

$$\begin{aligned}
P_v &= \frac{\beta^{2\alpha+1} e^{-\rho T_{v,x_0}} \gamma(\alpha, T_{v,x_0}(\beta - \rho))}{(\alpha\rho + \beta)(\beta - \rho)^{2\alpha} \Gamma(\alpha)} + \frac{\Gamma(\alpha, \beta T_{v,x_0})}{\Gamma(\alpha)} \\
&+ \frac{\rho}{\alpha\rho + \beta} \sum_{m=0}^{\alpha-1} \sum_{k=0}^m \frac{(\beta T_{v,x_0})^{\alpha+k}}{\Gamma(\alpha+k+1)} e^{-\beta T_{v,x_0}} \{1 - (\rho - \beta)^{m-\alpha}\}. \quad (24)
\end{aligned}$$

Proof. Note that $\gamma(\alpha, x)$ and $\Gamma(\alpha, x)$ can be represented as finite series when the shape parameter α is a positive integer value as shown in [32, Equation. 3.351-2]. In other words, we have:

$$\gamma(\alpha, x) = \Gamma(\alpha) \left(1 - \sum_{n=0}^{\alpha-1} \frac{x^n e^{-x}}{n!} \right), \Gamma(\alpha, x) = \Gamma(\alpha) \sum_{n=0}^{\alpha-1} \frac{x^n e^{-x}}{n!}. \quad (25)$$

Using (25), $\mathbb{P}[T_{\text{int}} \geq a + T_{v,x_0} - x - X_k]$ in (41) can be obtained as follows:

$$\begin{aligned}
&\mathbb{P}[T_{\text{int}} \geq a + T_{v,x_0} - x - X_k] \\
&= \frac{\beta^\alpha e^{-\rho(a+T_{v,x_0}-x)}}{(\beta-\rho)^\alpha} \left\{ 1 - \sum_{m=0}^{\alpha-1} \frac{(\beta-\rho)^m}{m!} (a+T_{v,x_0}-x)^m e^{-\frac{\beta}{\rho}} \right\} \\
&+ \sum_{m=0}^{\alpha-1} \frac{\beta^m}{m!} (a+T_{v,x_0}-x)^m e^{-\beta(a+T_{v,x_0}-x)}. \quad (26)
\end{aligned}$$

When computing $\mathbb{E}[T_k^v]$ in (40), for obtaining $E_1(x)$, the integral of (26), we can first derive the following:

$$\begin{aligned}
&\int_0^\infty \mathbb{P}[T_{\text{int}} \geq a + T_{v,x_0} - x - X_k] da \\
&= \int_0^\infty \left[\frac{\beta^\alpha e^{-\rho(a+T_{v,x_0}-x)}}{(\beta-\rho)^\alpha} - \left\{ \sum_{m=0}^{\alpha-1} \left(\frac{\beta}{(\beta-\rho)} \right)^\alpha \frac{(\beta-\rho)^m}{m!} - \frac{\beta^m}{m!} \right\} \times (a+T_{v,x_0}-x)^m e^{-\beta(a+T_{v,x_0}-x)} \right] da \\
&= \frac{\beta^\alpha e^{-\rho(T_{v,x_0}-x)}}{\rho(\beta-\rho)^\alpha} - \sum_{m=0}^{\alpha-1} \frac{\Gamma(m+1, \beta(T_{v,x_0}-x))}{\beta m!} \\
&\quad \times \{1 - (1 - \rho/\beta)^{m-\alpha}\}, \quad (27)
\end{aligned}$$

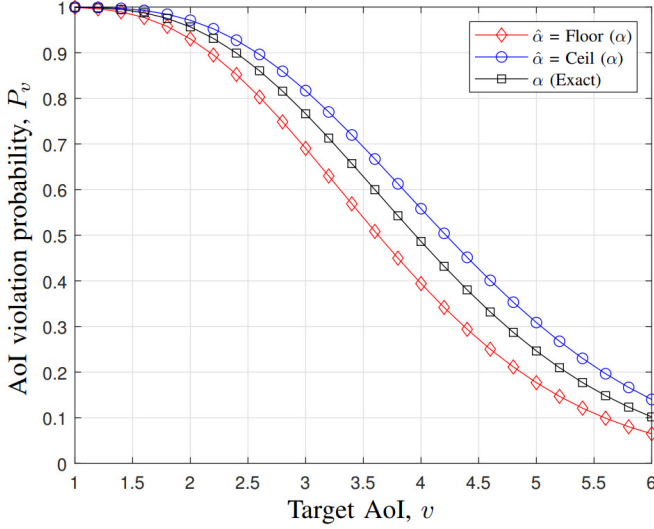


Fig. 4. AoI violation probability P_v as a function of a target AoI v for different shape parameters.

where the last equation is obtained by substituting k for $a + T_{v,x_0} - x$ and (42). Then, using (27), $E_1(x)$ can be obtained by

$$\begin{aligned} & \int_0^{T_{v,x_0}} \int_0^\infty \mathbb{P}[T_{\text{int}} \geq a + T_{v,x_0} - x - X_k] f_{X_{k-1}}(x) \, dx \, da \\ & \stackrel{(a)}{=} \frac{e^{-\rho T_{v,x_0}} \beta^{2\alpha} \gamma(\alpha, T_{v,x_0}(\beta - \rho))}{\rho \Gamma(\alpha) (\beta - \rho)^{2\alpha}} + \sum_{m=0}^{\alpha-1} \sum_{k=0}^m \frac{\beta^{\alpha+k-1} T_{v,x_0}^{\alpha+k}}{\Gamma(\alpha + k + 1)} \\ & \quad \times e^{-\beta T_{v,x_0}} \{1 - (1 - \rho/\beta)^{m-\alpha}\}, \end{aligned} \quad (28)$$

where (a) follows from the representation of $\gamma(\alpha, x)$ in (25) and the fact that a beta function $B(a, b)$ is the same as $\Gamma(a)\Gamma(b)/\Gamma(a+b)$ [32, Equation 8.384-1]. From (21), (40), (49), and (28), P_v with integer α can be obtained as (24). \square

Remark 1. From Corollary 1, we can see that P_v becomes one as the target STP ζ approaches one (i.e., $\zeta = 1$) since $T_{v,x_0} = (v - T_{\text{tx},x_0})^+$ approaches zero. This means that, in order to satisfy a higher target STP, the AoI violation will always happen because the transmission latency T_{tx,x_0} becomes large. Hence, we can see that a higher target STP does not always guarantee a lower AoI violation probability.

For the case of non-integer α , P_v in (24) can serve as an upper or lower bound of the AoI violation probability by using $\hat{\alpha} = \text{Ceil}(\alpha)$ or $\text{Floor}(\alpha)$ instead of α , respectively, where $\text{Ceil}(\cdot)$ and $\text{Floor}(\cdot)$ are the ceil and floor functions. This is because the complementary cumulative distribution function (CCDF) of the consensus latency can be upper bounded by the one with a higher shape parameter under the same rate parameter, and vice versa.

In Fig. 4, we compare the result of Corollary 1 as a function of v for target STP $\zeta = 0.5$. The shape parameter ($\alpha = 5.55$) is mapped to integers by the ceil and floor function. As shown in Fig. 4, we first observe that the three results show a similar trend. We can also see that the result of Corollary 1 can be the

upper or lower bound of Theorem 1 as discussed in Remark 1.

We now derive the PAoI violation probability, which is the probability that the PAoI is larger than or equal to a target value v , i.e., $P_{p^v} = \mathbb{P}[\Delta_{p,k} \geq v]$. This metric is particularly useful for a system that must maintain the worst-case AoI below a certain value as much as possible. In the following lemma, we analyze P_{p^v} .

Lemma 2. In BeMN, the PAoI violation probability P_{p^v} is given by

$$\begin{aligned} P_{p^v} = 1 - \frac{\beta^{2\alpha}}{\Gamma(\alpha)^2} \sum_{n=0}^{\infty} \sum_{k=0}^{\infty} \frac{T_{v,x_0}^{2\alpha+n+k}}{n!k!(\alpha+n)} B(\alpha+n+1, \alpha+k) \\ \times \{(-\beta)^{n+k} - e^{-\rho T_{v,x_0}} (\rho - \beta)^{n+k}\}, \end{aligned} \quad (29)$$

where $T_{v,x_0} = (v - T_{\text{tx},x_0})^+$.

Proof. From (14), the cumulative distribution function (CDF) of $\Delta_{p,k}$ is defined as

$$\begin{aligned} F_{\Delta_{p,k}}(v) &= \mathbb{P}[T_{\text{eff},k} + T_{\text{tot},k} \leq v] \\ &\stackrel{(a)}{=} \mathbb{P}[X_{k-1} + X_k + T_{\text{int}} + T_{\text{tx},x_0} \leq v], \end{aligned} \quad (30)$$

where (a) is from (1) and (13). We then have

$$\begin{aligned} F_{\Delta_{p,k}}(v) &= \int_0^{T_{v,x_0}} \mathbb{P}[x + X_k + T_{\text{int}} \leq v - T_{\text{tx},x_0}] f_{X_{k-1}}(x) \, dx \\ &= \int_0^{T_{v,x_0}} \int_0^{T_{v,x_0}-x} \{1 - e^{-\rho(T_{v,x_0}-x-x')}\} f_{X_k}(x') f_{X_{k-1}}(x) \, dx' \, dx \\ &= \frac{1}{\Gamma(\alpha)} \int_0^{T_{v,x_0}} \left[\gamma(\alpha, \beta(T_{v,x_0} - x)) - \frac{\beta^\alpha e^{-\rho(T_{v,x_0}-x)}}{(\beta - \rho)^\alpha} \right. \\ & \quad \left. \times \gamma(\alpha, (\beta - \rho)(T_{v,x_0} - x)) \right] f_{X_{k-1}}(x) \, dx. \end{aligned} \quad (31)$$

Using the Taylor series of $\exp(-\beta(T_{v,x_0} - x))$ and (44), $F_{\text{PAoI}_k}(v)$ in (31) can be given by

$$\begin{aligned} F_{\Delta_{p,k}}(v) &= \frac{\beta^{2\alpha}}{\Gamma(\alpha)^2} \sum_{n=0}^{\infty} \sum_{k=0}^{\infty} \left[\frac{1}{n!k!(\alpha+n)} \int_0^{T_{v,x_0}} (T_{v,x_0} - x)^n x^{\alpha+k-1} \right. \\ & \quad \left. \times \{(-\beta)^{n+k} - e^{-\rho T_{v,x_0}} (\rho - \beta)^{n+k} (T_{v,x_0} - x)^\alpha \, dx\} \right]. \end{aligned} \quad (32)$$

Using $\int_0^\alpha x^{\beta-1} (\alpha - x)^{m-1} \, dx = \alpha^{m+\beta-1} B(m, \beta)$ [32, Equation 3.191-1] and (2), $F_{\text{PAoI}_k}(v)$ in (32) is given by

$$\begin{aligned} F_{\Delta_{p,k}}(v) &= \frac{\beta^{2\alpha}}{\Gamma(\alpha)^2} \sum_{n=0}^{\infty} \sum_{k=0}^{\infty} \frac{T_{v,x_0}^{2\alpha+n+k}}{n!k!(\alpha+n)} B(\alpha+n+1, \alpha+k) \\ & \quad \times \{(-\beta)^{n+k} - e^{-\rho T_{v,x_0}} (\rho - \beta)^{n+k}\}. \end{aligned} \quad (33)$$

By taking the complement rule to (33), we obtain P_{p^v} as (29). \square

Lemma 2 can show the distribution of the worst-case of data freshness during update intervals. This result can be used to control the tail of the worst-case AoI, especially with applications that require a strict threshold of data freshness.

TABLE II. Average estimated shape and rate parameters (α, β) of the consensus latency distribution and the average KS statistics for different target STP ζ and block size B .

ζ	Average estimate (α, β)	Average latency/SD	Average skewness	Average KS statistics
0.3	(5.64, 3.01)	2.42/0.95	0.093	0.0732
0.4	(5.94, 2.45)	2.42/0.92	0.086	0.0623
0.5	(5.39, 2.85)	2.17/0.87	0.095	0.0506
0.6	(5.42, 2.84)	1.90/0.76	0.097	0.0504
0.7	(7.18, 3.73)	1.92/0.67	0.071	0.0462
0.8	(7.71, 4.12)	1.87/0.63	0.066	0.0423
0.9	(7.50, 4.35)	1.73/0.60	0.068	0.0369
1.0	(6.57, 3.82)	1.76/0.76	0.085	0.0532

TABLE III. Average estimated shape and rate parameters (α, β) of the consensus latency distribution and the average KS statistics for different timeout T .

T	Average estimate (α, β)	Average latency/SD	Average skewness	Average KS statistics
0.5	(2.74, 0.89)	3.08/2.00	0.194	0.0420
0.6	(4.26, 2.04)	2.10/1.07	0.122	0.0452
0.7	(8.28, 5.40)	1.53/0.54	0.061	0.0494
0.75	(6.78, 5.19)	1.30/0.47	0.076	0.0489
1.0	(6.96, 4.65)	1.50/0.54	0.075	0.0588
1.25	(9.62, 5.37)	1.79/0.55	0.053	0.0446
1.50	(9.86, 5.20)	1.89/0.56	0.052	0.0603
2.0	(6.79, 3.62)	1.87/0.66	0.075	0.0535
2.5	(5.64, 3.01)	1.97/0.72	0.091	0.0497
3.0	(5.42, 2.84)	1.89/0.76	0.097	0.0504
3.5	(5.39, 2.85)	1.89/0.75	0.091	0.0503

V. EXPERIMENTAL AND NUMERICAL RESULTS

In this section, we present experimental and numerical results to verify the analysis of the AoI violation probability P_v and to show the impact of BeMN parameters, i.e., target STP ζ , block size B , and timeout T , on data freshness.

A. Simulation Setup and KS Test

For our simulations, unless otherwise specified, we use $\rho_s = 15$, $P = 1$ W, $N_0 = -100$ dBm, $W = 1$ MHz, $D = 500$ kb, $\lambda = 0.0001$ (BS/km²), $l = 37$ m, $\zeta = 0.6$, $B = 20$, and $T = 3$. We implement an HLF platform with version 1.3 [17] on one physical machine with Intel(R) Xeon W-2155 @ 3.30GHz with 16 GB of RAM. The established HLF consists of one peer and two committing peers. Note that the committing peers only verify new blocks conveyed from the ordering service. We generate transactions to update a certain target key-value, which occupies 30 percent of the whole generated transactions. We measure the consensus latency of the generated target transactions with varying BeMN parameters. To investigate the effect of each parameter, we fit statistical distribution of thousand transactions for different BeMN parameters. Note that we use the maximum likelihood estimation method introduced in Section III-B. The accuracy

B	Average estimate (α, β)	Average latency/SD	Average skewness	Average KS statistics
3	(1.62, 0.30)	5.71/4.03	0.342	0.0831
5	(2.90, 1.38)	2.16/1.25	0.182	0.0333
7	(4.35, 2.58)	1.70/0.85	0.121	0.0498
10	(5.24, 3.30)	1.59/0.74	0.099	0.0495
12	(5.81, 3.66)	1.58/0.63	0.074	0.0382
15	(6.95, 3.85)	1.80/0.65	0.074	0.0381
20	(5.42, 2.84)	1.90/0.76	0.097	0.0504
25	(4.85, 2.36)	2.05/0.86	0.107	0.0604

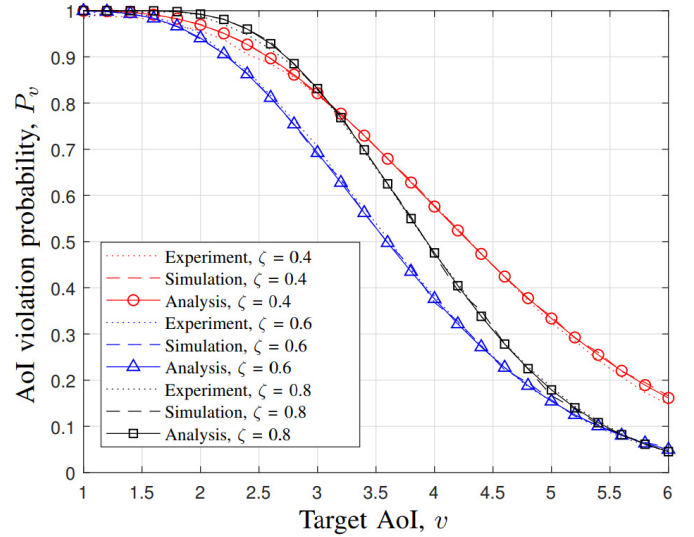


Fig. 5. AoI violation probability P_v as a function of a target AoI v for different target STPs ζ .

of the consensus latency modeling is investigated by using the KS test in the following.

The KS test returns the absolute value of the largest discrepancy between an empirical and theoretical cumulative distribution, known as the KS statistic [33]. A smaller KS statistic means a higher accuracy of the modeling. The KS test compares the KS statistic with a critical value, which is determined by the number of samples and a significance level. If the KS statistic is smaller than the critical value, it is seen as a reasonable theoretical model for the empirical distribution. From the generated transactions above, the corresponding estimated parameters (α, β) of the consensus latency and the KS statistics with a significance level of 0.01 are averaged over five runs and presented in Tables II and III. We also present the average standard deviation (SD) and the skewness of the measured consensus latencies from the experiments. Note that the critical value of the KS test for 1000 samples is 0.0515.

In Figs. 5, 6, and 7, we compare the analytical results with the simulation and the experimental results while varying the BeMN parameters as a function of v . In the simulation results, P_v is calculated by generating the consensus latencies using

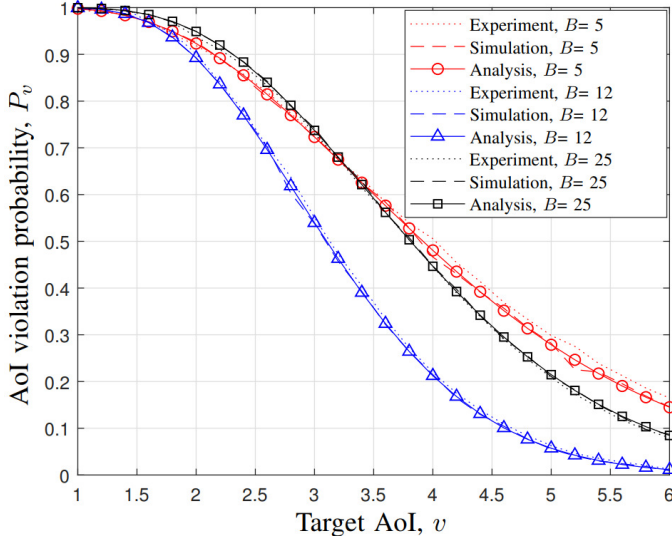


Fig. 6. AoI violation probability P_v as a function of target AoI v for different block size B .

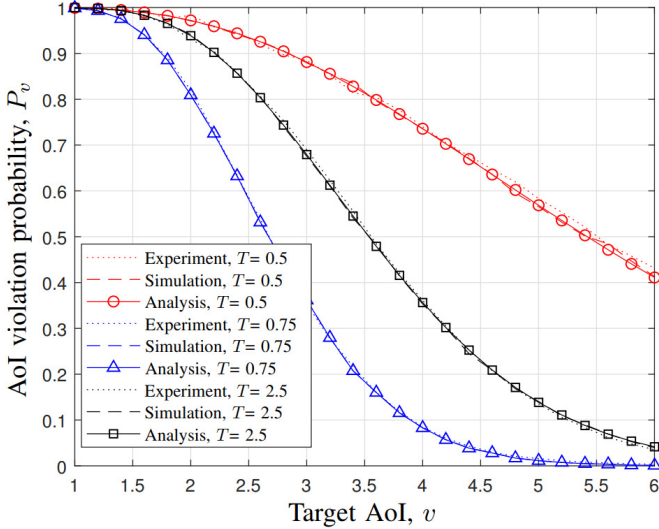


Fig. 7. AoI violation probability P_v as a function of target AoI v for different timeout T .

the modeled Gamma distribution. In the experimental results, we calculate P_v by using the measured consensus latencies in the established HLF platform.

Figure 5 presents P_v for the simulation and the experimental results as a function of v for $\zeta = 0.4, 0.6$, and 0.8 . We can first observe that the analytical and simulation results show a good match. We also observe that the analytical results match the experimental results, obtained from the HLF platform. Note that for $\zeta = 0.4$, the experimental results also match well with the analytical results although the KS statistic of this case is 0.0623, which is larger than the critical value 0.0515 (see Table II). This is because the distribution of the consensus latency and its modeled distribution have similar statistical properties. Specifically, from Table II, we can see that the average latency, the average SD, and the skewness of the measured latencies in the experiments are

2.42, 0.92, and 0.086, respectively. These are similar to the values calculated from the modeled distribution, which are $\frac{\alpha}{\beta} = 2.42$, $\frac{\sqrt{\alpha}}{\beta} = 0.98$, and $\frac{2}{\sqrt{\alpha}} = 0.082$. Therefore, our AoI analysis can capture the actual data freshness in BeMN. In addition, when the target AoI v is small (e.g., $v < 3$), the value of the AoI violation probability P_v for $\zeta = 0.4$ is less than the case in which $\zeta = 0.8$. This is because the transmission latency T_{tx,x_0} increases as ζ becomes larger, and, thus it becomes difficult to complete the status update within a short time for high ζ . On the other hand, when v is large (e.g., $v \geq 3$), P_v for $\zeta = 0.4$ is higher than the case in which $\zeta = 0.8$. In this case, most status updates can be performed without violating the large target AoI v . Hence, the number of successfully received packets becomes more important than reducing T_{tx,x_0} to maintain low P_v .

Figure 6 shows the analytical, simulation, and experimental results of P_v as a function of v for $B = 5, 12$, and 25 . For small v (e.g., $v < 3$), the value of the AoI violation probability P_v for $B = 5$ is lower than the case in which $B = 25$. However, this relationship is reversed when v is large (e.g., $v \geq 3$). This is because the consensus latency distributions of the both cases show different statistical characteristics. From Table II, we observe that P_v for $B = 5$ yields larger SD and skewness than the case in which $B = 25$. Thus, the distribution of $B = 5$ is concentrated more on the left, and it has a larger tail probability compared with $B = 25$.

Figure 7 presents the three results of P_v as a function of v for $T = 0.5, 0.75$, and 2.5 . We can see that the AoI violation probability P_v for $T = 0.5$ achieves the largest mean latency, SD and skewness. Although its distribution is highly skewed to the left, it is mostly concentrated near the large mean value. Moreover, the high SD results in a large tail probability, which leads to larger P_v than the other cases.

As shown in Figs. 5, 6, and 7, having a smaller (or larger) value for the target STP, block size, or timeout does not always guarantee a lower (or larger) AoI violation probability. This is due to the conflicting effects of those parameters on the transmission and the consensus latencies. These effects will be discussed more in the following subsection.

B. Impact of BeMN Parameters

Figure 8 shows P_v , P_{pv} , and $\bar{\Delta}$ for different values of ζ with $v = 5.5$, and $D = 250$ kb. From Fig. 8, we can observe that P_v , P_{pv} , and $\bar{\Delta}$ have a similar trend according to ζ . In particular, all metrics first decrease and then increase with ζ . This is because when ζ is small, there are many outages in the packet transmission, so the status is seldom updated, which increases the AoI. Hence, in this case, the AoI-related performance becomes better as ζ increases. However, as ζ increases, the transmission latency T_{tx,x_0} also increases. Hence, when ζ is higher than a certain value, the packets are reliably received at the HLF, but the AoI-related performance degrades with ζ due to the longer transmission latency.

Figure 9 presents P_v , P_{pv} , and $\bar{\Delta}$ for different values of B with $v = 5.5$ and $D = 250$ kb. As shown in Fig. 9, all metrics, P_v , P_{pv} , and $\bar{\Delta}$, first decrease and then increase with B . When B is small, the block generation rate exceeds the block

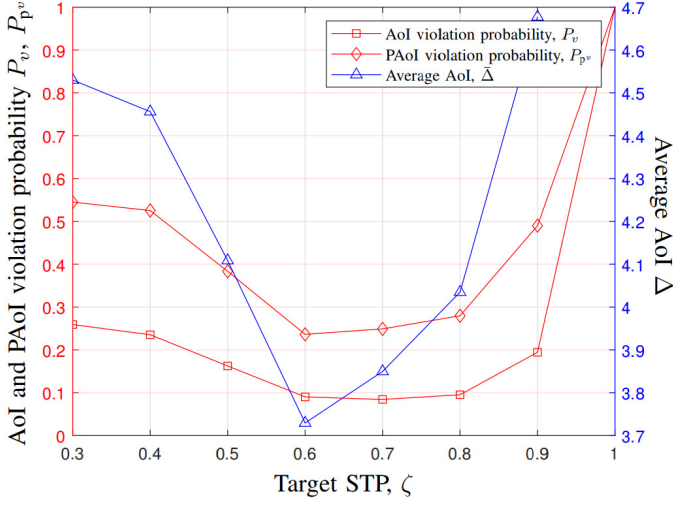


Fig. 8. AoI violation probability P_v , PAoI violation probability P_{p^v} , and average AoI $\bar{\Delta}$ as a function of target STP ζ for the target AoI $v = 5.5$ and the data size $D = 250$ kb.

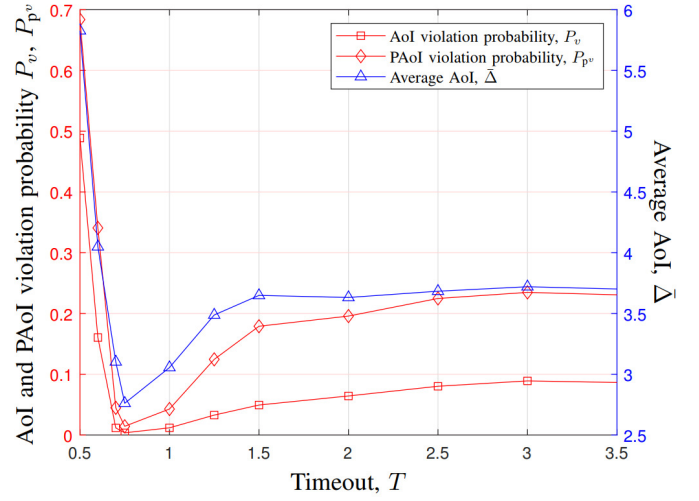


Fig. 10. AoI violation probability P_v , PAoI violation probability P_{p^v} , and average AoI $\bar{\Delta}$ as a function of timeout T for the target AoI $v = 5.5$ and the data size $D = 250$ kb.

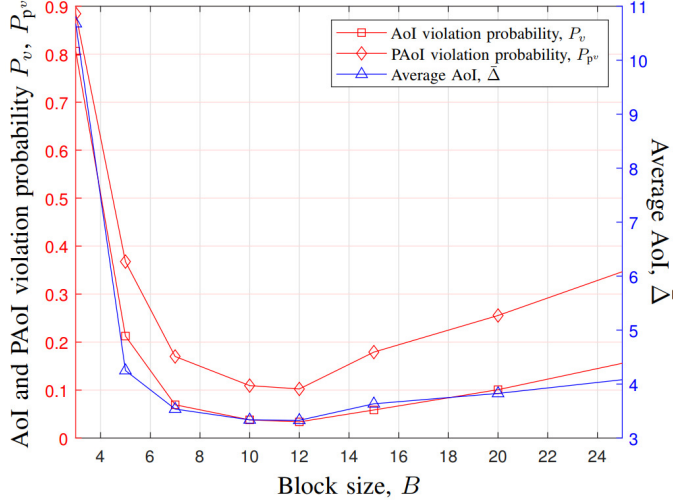


Fig. 9. AoI violation probability P_v , PAoI violation probability P_{p^v} , and average AoI $\bar{\Delta}$ as a function of block size B for the target AoI $v = 5.5$ and the data size $D = 250$ kb.

commitment rate in the validation phase, which increases the consensus latency. In particular, the time to commit the m blocks of size $\frac{B}{m}$ is always larger than the time to commit the block of size B for $m \geq 1$ [34]. Hence, in this case, the AoI-related performance improves as B increases. However, as B keeps increasing, the amount of time that a transaction has to wait in a block also increases. Therefore, when B exceeds a certain value, the AoI-related performance decreases with B due to longer waiting time in the ordering phase.

In Fig. 10, we present P_v , P_{p^v} , and $\bar{\Delta}$ for different values of T with $v = 5.5$ and $D = 250$ kb. We can see that all metrics first decrease and then increase with T . For small T , the block generation rate in the ordering phase is larger than peers' block commitment rate. Hence, the consensus latency increases, which increases the AoI. In this case, the AoI-

related performance improves as T increases. Nevertheless, as T increases, a transaction has to wait longer until the timeout expires. Thus, the AoI-related performance degrades with T because of the longer latency in the ordering phase. When $T \times \rho \geq B$, most of blocks can be generated before the timeout expires, so the effect of T almost vanishes. Therefore, the AoI-related performance does not change with T any more in this case.

VI. CONCLUSION

In this paper, we have studied the statistical characteristics of the AoI in BeMN. By considering both the transmission latency and the consensus latency, we have presented closed-form expressions for the average AoI, the AoI violation probability, and the PAoI violation probability. We have also obtained an upper and lower bound of the AoI violation probability in a simpler form. Further, we have validated our analytical results through the simulations and experiments after constructing the HLF platform. We have shown that the analytical results can precisely provide the distribution of the data freshness in BeMN. We have also investigated the effects of BeMN parameters on the AoI violation probability. Our results show that: 1) as the target STP increases, the transmission latency becomes longer while the number of reliably received packets for status updates increases, and 2) as the block size or the timeout in an HLF network becomes larger, the ordering phase latency increases while the latency in the validation phase decreases due to a smaller load from a lower block generation rate. We have shown that BeMN should be properly designed by considering the conflicting effects of the BeMN parameters on the AoI. The proposed framework can thus be a useful guideline for the design of BeMN.

APPENDIX

A. Proof of Proposition 1

From (7) and (8), $\bar{\epsilon}_{x_0}$ can be represented as

$$\bar{\epsilon}_{x_0} = \max \{ \epsilon \mid \mathbb{P} [\gamma_{x_0} \geq 2^{\frac{\epsilon}{W}} - 1] \geq \zeta \}. \quad (34)$$

From (5), $\mathbb{P} [\gamma_{x_0} \geq 2^{\frac{\epsilon}{W}} - 1]$ in (34) can be given by

$$\mathbb{P} [\gamma_{x_0} \geq 2^{\frac{\epsilon}{W}} - 1] = \exp \left(-\frac{l^n}{P} N_0 W \theta(\epsilon) \right) \mathbb{E}_{I_{x_0}} \left[\exp \left(-\frac{l^n}{P} I_{x_0} \theta(\epsilon) \right) \right], \quad (35)$$

where $\theta(\epsilon) = 2^{\epsilon/W} - 1$ by using the CDF of the exponential random variable h_{x_0} .

With the assumption that the distribution of interfering sources follows the HPPP,³ the Laplace transform of I_{x_0} can be given by [36, Equation 3.21]

$$\mathcal{L}_{I_{x_0}}(s) = \exp \left\{ -\lambda \pi s^{2/n} \frac{2\pi}{n \sin(2\pi/n)} \right\}. \quad (36)$$

Using (36), (35) can be derived as follows

$$\begin{aligned} \mathbb{P} [\gamma_{x_0} \geq 2^{\frac{\epsilon}{W}} - 1] &= \exp \left(-\frac{l^n}{P} N_0 W \theta(\epsilon) \right) \\ &\quad \times \exp \left(-\lambda \pi^2 \frac{2l^2 \theta(\epsilon)^{2/n}}{nP^{2/n} \sin(2\pi/n)} \right). \end{aligned} \quad (37)$$

By substituting (37) into (34), $\bar{\epsilon}_{x_0}$ in (34) can be given by

$$\bar{\epsilon}_{x_0} = \max \left\{ \epsilon \mid \exp \left(-\frac{l^n}{P} N_0 W \theta(\epsilon) - \frac{2\lambda \pi^2 l^2 \theta(\epsilon)^{2/n}}{nP^{2/n} \sin(2\pi/n)} \right) \geq \zeta \right\}. \quad (38)$$

Since p_c is a decreasing function of ϵ , the value of $\bar{\epsilon}_{x_0}$ is the largest ϵ that satisfies $p_c \geq \zeta$. Hence, $\bar{\epsilon}_{x_0}$ in (38) is the same as the one satisfying (9).

B. Proof of Theorem 1

In (21), the expectation of T_k^v is given by

$$\mathbb{E}[T_k^v] = \int_0^\infty \mathbb{P}[T_k^v \geq z] dz. \quad (39)$$

Using (22) and (39), $\mathbb{E}[T_k^v]$ can be represented by

$$\begin{aligned} \mathbb{E}[T_k^v] &= \int_0^{T_{v,x_0}} \underbrace{\int_0^\infty \mathbb{P}[x + X_k + T_{\text{int}} - T_{v,x_0} \geq z] f_{X_{k-1}}(x) dz}_{E_1(x)} dx \\ &\quad + \int_{T_{v,x_0}}^\infty \underbrace{\int_0^\infty \mathbb{P}[X_k + T_{\text{int}} \geq z] f_{X_{k-1}}(x) dz}_{E_2(x)} dx, \end{aligned} \quad (40)$$

where $f_{X_{k-1}}(x)$ is in (2). In (40), $\mathbb{P}[x + X_k + T_{\text{int}} - T_{v,x_0} \geq z]$ can be given by

$$\mathbb{P}[T_{\text{int}} \geq z + T_{v,x_0} - x - X_k]$$

³Note that the distribution of the interfering sources does not follow HPPP because their locations are dependent. Nevertheless, this dependency is shown to be weak in [35].

$$\begin{aligned} &= \int_0^\infty \mathbb{P}[T_{\text{int}} \geq z + T_{v,x_0} - x - w | X_k = w] f_{X_k}(w) dw \\ &= \int_0^{z+T_{v,x_0}-x} e^{-\rho(z+T_{v,x_0}-x-w)} f_{X_k}(w) dw \\ &\quad + \int_{z+T_{v,x_0}-x}^\infty f_{X_k}(w) dw \\ &= \frac{\beta^\alpha e^{-\rho(z+T_{v,x_0}-x)}}{\Gamma(\alpha)} \frac{\gamma(\alpha, (\beta-\rho)(z+T_{v,x_0}-x))}{(\beta-\rho)^\alpha} \\ &\quad + \frac{\Gamma(\alpha, \beta(z+T_{v,x_0}-x))}{\Gamma(\alpha)}, \end{aligned} \quad (41)$$

where the second equation is obtained from the fact that $\mathbb{P}[T_{\text{int}} \geq z + T_{v,x_0} - x - X_k | X_k]$ is always one when X_k is larger than $z + T_{v,x_0} - x$ and using the exponential distribution of T_{int} . In (41), $\gamma(\cdot, \cdot)$ and $\Gamma(\cdot, \cdot)$ are the lower and upper incomplete gamma functions, respectively, i.e.,

$$\gamma(\alpha, x) = \int_0^x t^{\alpha-1} e^{-t} dt \text{ and } \Gamma(\alpha, x) = \int_x^\infty t^{\alpha-1} e^{-t} dt. \quad (42)$$

Using (41), $E_1(x)$ in (40) can be obtained as

$$\begin{aligned} E_1(x) &= \int_0^\infty \left[\frac{\beta^\alpha e^{-\rho(z+T_{v,x_0}-x)} \gamma(\alpha, (\beta-\rho)(z+T_{v,x_0}-x))}{\Gamma(\alpha)(\beta-\rho)^\alpha} \right. \\ &\quad \left. + \frac{\Gamma(\alpha, \beta(z+T_{v,x_0}-x))}{\Gamma(\alpha)} \right] dz \\ &\stackrel{(a)}{=} \frac{\beta^\alpha}{\Gamma(\alpha)} \sum_{n=0}^\infty \frac{(\rho-\beta)^n}{n! (\alpha+n)} \int_0^\infty (z+T_{v,x_0}-x)^{\alpha+n} e^{-\rho(z+T_{v,x_0}-x)} dz \\ &\quad + \frac{1}{\Gamma(\alpha)} \int_0^\infty \int_{\beta(z+T_{v,x_0}-x)}^\infty t^{\alpha-1} e^{-t} dt dz \\ &\stackrel{(b)}{=} \underbrace{\frac{\beta^\alpha}{\Gamma(\alpha)} \sum_{n=0}^\infty \frac{(\rho-\beta)^n}{n! (\alpha+n)} \Gamma(\alpha+n+1, \rho(T_{v,x_0}-x))}_{f_1(x)} \\ &\quad + \underbrace{\frac{\Gamma(\alpha+1, \beta(T_{v,x_0}-x))}{\beta \Gamma(\alpha)}}_{f_2(x)} + \underbrace{\frac{(x-T_{v,x_0})}{\Gamma(\alpha)} \Gamma(\alpha, \beta(T_{v,x_0}-x))}_{f_3(x)}, \end{aligned} \quad (43)$$

where (a) follows from the fact that the lower incomplete Gamma function $\gamma(\alpha, x)$ can be represented as [32, Equation 8.354-1]

$$\gamma(\alpha, x) = \sum_{n=0}^\infty \frac{(-1)^n x^{\alpha+n}}{n! (\alpha+n)}, \quad (44)$$

and (b) is obtained by changing the order of the integral and (42). Using (43), the integral of $E_1(x)$ in (40) can be represented as

$$\int_0^{T_{v,x_0}} E_1(x) dx = \int_0^{T_{v,x_0}} \{f_1(x) + f_2(x) + f_3(x)\} f_{X_{k-1}}(x) dx, \quad (45)$$

where $f_i(x)$ are defined in (43) for $i \in \{1, 2, 3\}$. In (45), the first term can be given by

$$\int_0^{T_{v,x_0}} f_1(x) f_{X_{k-1}}(x) dx$$

$$\begin{aligned}
&\stackrel{(a)}{=} \frac{\beta^{2\alpha}}{\Gamma(\alpha)^2} \sum_{n=0}^{\infty} \frac{(\rho - \beta)^n}{n! (\alpha + n) \rho^{\alpha+n+1}} \int_0^{T_{v,x_0}} \left[\Gamma(\alpha + n + 1) \right. \\
&\quad \left. - \sum_{k=0}^{\infty} \frac{(-1)^k \{\rho(T_{v,x_0} - x)\}^{\alpha+n+k+1}}{k! (\alpha + n + k + 1)} \right] x^{\alpha-1} e^{-\beta x} dx \\
&\stackrel{(b)}{=} \frac{\beta^{2\alpha}}{\Gamma(\alpha)^2} \sum_{n=0}^{\infty} \frac{(\rho - \beta)^n}{n! (\alpha + n) \rho^{\alpha+n+1}} \left[\frac{\Gamma(\alpha + n + 1)}{\beta^\alpha} \gamma(\alpha, \beta T_{v,x_0}) \right. \\
&\quad \left. - \sum_{k=0}^{\infty} \frac{(-1)^k (\rho T_{v,x_0})^{\alpha+n+k+1}}{k! (\alpha + n + k + 1)} T_{v,x_0}^\alpha B(\alpha + n + k + 2, \alpha) \right. \\
&\quad \left. \times {}_1F_1(\alpha; 2\alpha + n + k + 2; \beta T_{v,x_0}) \right], \quad (46)
\end{aligned}$$

where $B(\cdot, \cdot)$ is the beta function, and ${}_1F_1(\cdot; \cdot; \cdot)$ is the confluent hypergeometric function. In (46), (a) is obtained since $\Gamma(\alpha, x) = \Gamma(\alpha) - \gamma(\alpha, x)$, and (b) follows from [32, Equation 3.383-1]. Similarly, in (45), the second term can be obtained as

$$\begin{aligned}
&\int_0^{T_{v,x_0}} f_2(x) f_{X_{k-1}}(x) dx \\
&= \frac{\beta^{2\alpha}}{\Gamma(\alpha)^2} \int_0^{T_{v,x_0}} \left[\Gamma(\alpha + 1) - \sum_{n=0}^{\infty} \frac{(-\beta)^n (T_{v,x_0} - x)^{\alpha+n+1}}{n! (\alpha + n + 1)} \right] \\
&\quad \times x^{\alpha-1} e^{-\beta x} dx \\
&= \frac{\alpha \gamma(\alpha, \beta T_{v,x_0})}{\beta \Gamma(\alpha)} - \sum_{n=0}^{\infty} \frac{(-1)^n (\beta T_{v,x_0})^{2\alpha+n}}{n! (\alpha + n + 1)} B(\alpha + n + 2, \alpha) \\
&\quad \times \frac{T_{v,x_0}}{\Gamma(\alpha)^2} {}_1F_1(\alpha; 2\alpha + n + 2; -\beta T_{v,x_0}). \quad (47)
\end{aligned}$$

The third term in (45) is given by

$$\begin{aligned}
&\int_0^{T_{v,x_0}} f_3(x) f_{X_{k-1}}(x) dx \\
&\stackrel{(a)}{=} -\frac{\beta^\alpha}{\Gamma(\alpha)^2} \int_0^{T_{v,x_0}} k \Gamma(\alpha, \beta k) (T_{v,x_0} - k)^{\alpha-1} e^{-\beta(T_{v,x_0}-k)} dk \\
&\stackrel{(b)}{=} -\frac{\beta^\alpha}{\Gamma(\alpha)^2} \int_0^{T_{v,x_0}} \left\{ \Gamma(\alpha) - \sum_{n=0}^{\infty} \frac{(-1)^n (\beta k)^{\alpha+n}}{n! (\alpha + n)} \right\} \\
&\quad \times k (T_{v,x_0} - k)^{\alpha-1} e^{-\beta(T_{v,x_0}-k)} dk \\
&\stackrel{(c)}{=} -\frac{T_{v,x_0} (\beta T_{v,x_0})^\alpha e^{-\beta T_{v,x_0}}}{\Gamma(\alpha)} B(\alpha, 2) {}_1F_1(2; \alpha + 2; \beta T_{v,x_0}) \\
&\quad + \frac{T_{v,x_0} e^{-\beta T_{v,x_0}}}{\Gamma(\alpha)^2} \sum_{n=0}^{\infty} \frac{(-1)^n (\beta T_{v,x_0})^{2\alpha+n}}{n! (\alpha + n)} B(\alpha, \alpha + n + 2) \\
&\quad \times {}_1F_1(\alpha + n + 2; 2\alpha + n + 2; \beta T_{v,x_0}) \\
&\stackrel{(d)}{=} -\frac{T_{v,x_0} (\beta T_{v,x_0})^\alpha}{\Gamma(\alpha)} B(\alpha, 2) {}_1F_1(\alpha; \alpha + 2; -\beta T_{v,x_0}) \\
&\quad + \frac{T_{v,x_0}}{\Gamma(\alpha)^2} \sum_{n=0}^{\infty} \frac{(-1)^n (\beta T_{v,x_0})^{2\alpha+n}}{n! (\alpha + n)} B(\alpha, \alpha + n + 2) \\
&\quad \times {}_1F_1(\alpha; 2\alpha + n + 2; -\beta T_{v,x_0}), \quad (48)
\end{aligned}$$

where (a) is obtained by substituting k for $T_{v,x_0} - x$, (b) follows from (44), (c) is obtained by the similar steps, which are used in (46), and (d) stems from ${}_1F_1(a; b; z) = e^z {}_1F_1(b - a; b; -z)$ in [32, Equation 9.212-1].

Now, we derive the integral of $E_2(x)$ in (40). In the integral range of z , $X_k + T_{\text{int}} \geq 0$ holds. Hence, we have

$$\begin{aligned}
&\int_{T_{v,x_0}}^{\infty} E_2(x) dx = \int_{T_{v,x_0}}^{\infty} \int_0^{\infty} \mathbb{P}[X_k + T_{\text{int}} \geq z] dz f_{X_{k-1}}(x) dx \\
&\stackrel{(a)}{=} (\mathbb{E}[X_k] + \mathbb{E}[T_{\text{int}}]) \int_{T_{v,x_0}}^{\infty} f_{X_{k-1}}(x) dx \\
&= \left(\frac{\alpha}{\beta} + \frac{1}{\rho} \right) \frac{\Gamma(\alpha, \beta T_{v,x_0})}{\Gamma(\alpha)}, \quad (49)
\end{aligned}$$

where (a) is obtained since X_k and T_{int} are independent.

Finally, $\mathbb{E}[T_k^v]$ is the summation of (46), (47), (48), and (49). Note that $\mathbb{E}[T_k] = \mathbb{E}[X_k + T_{\text{int}}] = \frac{\alpha}{\beta} + \frac{1}{\rho}$. Therefore, we obtain P_v as the ratio of $\mathbb{E}[T_k^v]$ and $\mathbb{E}[T_k]$ as (23).

REFERENCES

- [1] M. Kim, S. Lee, C. Park, and J. Lee, "Age of information analysis in hyperledger fabric blockchain-enabled monitoring networks," in *Proc. IEEE Int. Conf. Commun.*, Montreal, Canada, Jun. 2021, pp. 1–6.
- [2] O. Novo, "Blockchain meets iot: An architecture for scalable access management in iot," *IEEE Internet Things J.*, vol. 5, no. 2, pp. 1184–1195, Apr. 2018.
- [3] S. Kaul, R. Yates, and M. Gruteser, "Real-time status: How often should one update?" in *Proc. IEEE Conf. on Computer Commun.*, Orlando, FL, USA, Mar. 2012, pp. 1–5.
- [4] M. Costa, M. Codreanu, and A. Enpremedes, "On the age of information in status update systems with packet management," *IEEE Trans. Inf. Theory*, vol. 62, no. 4, pp. 1897–1910, Apr. 2016.
- [5] L. Hang and D. Kim, "Design and implementation of an integrated IoT blockchain platform for sensing data integrity," *Sensors*, vol. 19, no. 10, p. 2228, May 2019.
- [6] L. D. Nguyen, A. E. Kalør, I. Leyva-Mayorga, and P. Popovski, "Design and implementation of an integrated IoT blockchain platform for sensing data integrity," *IEEE Commun. Mag.*, vol. 58, no. 6, pp. 77–83, Jun. 2020.
- [7] S. M. Alrubei, E. A. Ball, J. M. Rigelsford, and C. A. Willis, "Latency and performance analyses of real-world wireless iot-blockchain application," *IEEE Sensors J.*, vol. 20, no. 13, pp. 7372–7383, Jul. 2020.
- [8] M. Alaslani, F. Nawab, and B. Shihada, "Blockchain in IoT systems: End-to-end delay evaluation," *IEEE Internet Things J.*, vol. 6, no. 5, pp. 8332–8344, Oct. 2019.
- [9] A. Rovira-Suganes and A. Razi, "Optimizing the age of information for blockchain technology with applications to iot sensors," *IEEE Commun. Lett.*, vol. 24, no. 1, pp. 183–187, Jan. 2020.
- [10] D. Li, S. Wu, Y. Wang, J. Jiao, and Q. Zhang, "Age-optimal HARQ design for freshness-critical satellite-iot systems," *IEEE Internet Things J.*, vol. 7, no. 3, pp. 2066–2076, Jun. 2020.
- [11] B. Yu, Y. Cai, D. Wu, and Z. Xiang, "Average age of information in short packet based machine type communication," *IEEE Trans. Veh. Technol.*, vol. 69, no. 9, pp. 10306–10319, Sep. 2020.
- [12] A. Maatouk, M. Assaad, and A. Ephremides, "On the age of information in a csma environment," *IEEE/ACM Trans. Netw.*, vol. 28, no. 2, pp. 818–831, Feb. 2020.
- [13] M. A. Abd-Elmagid, N. Pappas, and H. S. Dhillon, "On the role of age of information in the internet of things," *IEEE Commun. Mag.*, vol. 57, no. 12, pp. 72–77, Dec. 2019.
- [14] X. Zheng, S. Zhou, Z. Jiang, and Z. Niu, "Closed-form analysis of non-linear age of information in status updates with an energy harvesting transmitter," *IEEE Trans. Wireless Commun.*, vol. 18, no. 8, pp. 4129–4142, Aug. 2019.
- [15] B. Zhou and W. Saad, "Minimum age of information in the internet of things with non-uniform status packet sizes," *IEEE Trans. Wireless Commun.*, vol. 19, no. 3, pp. 1933–1947, Mar. 2020.
- [16] C. Chaccour and W. Saad, "On the ruin of age of information in augmented reality over wireless terahertz (thz) networks," in *Proc. IEEE Global Telecomm. Conf.*, Dec. 2020, pp. 1–6.
- [17] <https://github.com/hyperledger/fabric/releases/tag/v1.3.0>.
- [18] M. Kuzlu, M. Pipattanasomporn, L. Gurses, and S. Rahman, "Performance analysis of a hyperledger fabric blockchain framework: Throughput, latency and scalability," in *Proc. IEEE Int. Conf. Blockchain (Blockchain)*, Atlanta, GA, USA, Jul. 2019, pp. 536–540.

- [19] E. Androulaki, A. Barger, V. Bortnikov, C. Cachin, K. Christidis, A. De Caro, D. Enyeart, C. Ferris, G. Laventman, Y. Manevich *et al.*, "Hyperledger Fabric: a distributed operating system for permissioned blockchains," in *Proc. EuroSys Conference*, Apr. 2018, pp. 1–15.
- [20] S. Lee, M. Kim, J. Lee, R.-H. Hsu, and T. Q. S. Quek, "Is blockchain suitable for data freshness? age-of-information perspective," *IEEE Netw.*, pp. 96 – 103.
- [21] A. Ledeczi, T. Hay, P. Volgyesi, D. R. Hay, A. Nadas, and S. Jayaraman, "Wireless acoustic emission sensor network for structural monitoring," *IEEE Sensors J.*, vol. 9, no. 11, pp. 1370–1377, Nov. 2009.
- [22] I. Martin, T. O'Farrell, R. Aspey, S. Edwards, T. James, P. Loskot, T. Murray, I. Rutt, N. Selmes, and T. Baugé, "A high-resolution sensor network for monitoring glacier dynamics," *IEEE Sensors J.*, vol. 14, no. 11, pp. 3926–3931, Nov. 2014.
- [23] J. Zhao and R. Govindan, "Understanding packet delivery performance in dense wireless sensor networks," in *Proc. ACM SENSYS*, Nov. 2003, pp. 1–13.
- [24] A. Valehi and A. Razi, "Maximizing energy efficiency of cognitive wireless sensor networks with constrained Age of Information," *IEEE Trans. Cogn. Commun. Netw.*, vol. 3, no. 4, pp. 643–654, Dec. 2017.
- [25] S. Lee, M. Kim, J. Lee, R. Hsu, and T. Quek, "Latency modeling of hyperledger fabric for blockchain-enabled IoT networks," *arXiv:2102.09166*, 2021.
- [26] H. C. Thom, "A note on the gamma distribution," *Monthly Weather Review*, vol. 86, no. 4, pp. 117–122, 1958.
- [27] N. T. Ison, A. M. Feyerherm, and L. D. Bark, "Wet period precipitation and the gamma distribution," *Journal of Applied Meteorology*, vol. 10, no. 4, pp. 658–665, Aug. 1971.
- [28] J. W. Shin, J.-H. Chang, and N. S. Kim, "Statistical modeling of speech signals based on generalized gamma distribution," *IEEE Signal Process. Lett.*, vol. 12, no. 3, pp. 258–261, Mar. 2005.
- [29] C. Park and J. Lee, "Mobile edge computing-enabled heterogeneous networks," *IEEE Trans. Wireless Commun.*, vol. 20, no. 2, pp. 1038–1051, Oct. 2020.
- [30] Y. Sun, E. Uysal-Biyikoglu, R. D. Yates, C. E. Koksall, and N. B. Shroff, "Update or wait: How to keep your data fresh," *IEEE Trans. Inf. Theory*, vol. 63, no. 11, pp. 7492–7508, Nov. 2017.
- [31] J. P. Champati, H. Al-Zubaidy, and J. Gross, "On the distribution of age of information for the GI/GI/1/1 and GI/GI/1/2* systems: Exact expressions and bounds," in *Proc. IEEE Conf. on Computer Commun.*, Paris, France, Apr. 2019, pp. 37–45.
- [32] I. S. Gradshteyn and I. M. Ryzhik, *Table of integrals, series, and products*. Academic press, 2014.
- [33] A. H.-S. Ang and W. H. Tang, *Probability concepts in engineering planning and design: Emphasis on application to civil and environmental engineering*. Wiley, 2007.
- [34] P. Thakkar, S. Nathan, and B. Viswanathan, "Performance benchmarking and optimizing hyperledger fabric blockchain platform," in *Proc. IEEE Int. Symp. on Modeling, Analysis, and Simulation of Computer and Telecommunication Systems (MASCOTS)*, Milwaukee, WI, USA, Sep. 2018, pp. 1–13.
- [35] T. D. Novlan, H. S. Dhillon, and J. G. Andrews, "Analytical modeling of uplink cellular networks," *IEEE Trans. Wireless Commun.*, vol. 12, no. 6, pp. 2669–2679, Jun. 2013.
- [36] M. Haenggi and R. K. Ganti, *Interference in large wireless networks*. Now Publishers Inc, 2009.